Numerical and experimental investigation into the aerodynamic benefits of rotorcraft formation flight

Duivenvoorden, Ramon; Voskuijl, Mark; Morée, Lars; de Vries, Jan; van der Veen, Finbar

Numerical and Experimental Investigation into the Aerodynamic Benefits of Rotorcraft Formation Flight

Ramon Duivenvoorden
Graduate student
Delft University of Technology
Delft, The Netherlands

Mark Voskuijl
Professor
Netherlands Defence Academy
Den Helder, The Netherlands

Lars Morée
2nd Lieutenant
Royal Netherlands Air Force
Den Helder, The Netherlands

Jan de Vries
Assistant professor
Netherlands Defence Academy
Den Helder, The Netherlands

Finbar van der Veen
Cadet-Sergeant
Netherlands Defence Academy
Den Helder, The Netherlands

ABSTRACT

The use of formation flight to achieve aerodynamic benefit as applied to rotorcraft is, unlike its fixed-wing counterpart, an unproven principle. This document presents a proof-of-concept of rotorcraft formation flight through a numerical research study, supported by results from an independent wind-tunnel experiment. In both cases, two helicopters are placed in an echelon formation aligned on the advancing side of the main rotor, though they do not simulate directly comparable flight conditions. The vertical and lateral alignment is varied in order to observe the achievable reductions in main rotor power required during cruise flight. The wind-tunnel experiment data yields an estimated maximum total power reduction for the secondary aircraft of 24%, while the numerical models yield reductions between 20% and 34% dependent on flight velocity. Both experiments predict a higher potential for aerodynamic benefit than observed for fixed-wing formations, which is contributed to the asymmetric upwash profile in the rotor wake. Optimal lateral alignment of both experimental and numerical results is found to feature overlap of the rotor disk areas due to circular area effects. Experimental data shows an optimal vertical alignment of the secondary rotorcraft below the primary, due to wake displacement. This is not present in the numerical simulations as a result of the applied leader wake modeling.

NOTATION

D	Rotor diameter	$[m]$
M_θ, M_ϕ	Pitch and roll moments	$[Nm]$
$P_{req,MR}$	Main rotor power required	$[kW]$
R	Rotor radius	$[m]$
V	Flight velocity	$[m/s]$
$x/R, y/R, z/R$	Coordinate w.r.t. (leader) rotor hub	$[-]$
$\beta_0, \beta_{1c}, \beta_{1s}$	Flapping angles	$[deg]$
$\Gamma(y)/\Gamma_0$	Normalized vorticity distribution	$[-]$
$\theta_0, \theta_{1s}, \theta_{1c}, \theta_{0T}$	control angles	$[deg]$
$\theta_{body}, \phi_{body}, \psi_{body}$	Fuselage pitch, roll and yaw angles	$[deg]$
λ	Induced velocity	$[-]$
μ	Advance ratio	$[-]$

INTRODUCTION

The subject of formation flight for aerodynamic benefit is thoroughly examined for both bird flight and subsequently fixed-wing aircraft, all leading to the conclusion that large (induced) drag reductions are achievable across a formation of aircraft. The subject is however completely untouched regarding rotary wing vehicles, although the increased interest in rotorcraft in recent years certainly merits its investigation.

Presented at the VFS International 76th Annual Forum & Technology Display, Virginia Beach, Virginia, October 68, 2020. C

Background

The main principle of formation flight for aerodynamic benefit is the utilization of the upwash outboard of the wake of a primary aircraft by a secondary aircraft, which induces an additional angle of attack on the wing. This has the primary effect that the lift vector is tilted forward and thus provides a component counteracting drag. Since its first characterization by Weiselberger in 1914 (Ref. 1) this subject has matured from investigations on large formations of birds, most notably by Lissaman et al. (Ref. 2) and Hummel (Refs. 3, 4), to the application on full-scale passenger and cargo aircraft at practically feasible flight configurations, such as the extensive works by Ning et al. (Refs. 5, 6) and the experimental tests of NASA's Surfing Aircraft Vortices for Efficiency (SAVE) program (Ref. 7). All of these investigations consistently report induced drag reductions of the follower in a two-aircraft echelon formation at longitudinal separations of at least ten spans

of roughly 30-50%, which translates to 10-15% of total drag reduction.

Considering rotorcraft however, no such research has been published to date. Any research which considers the aerodynamic interference between two rotorcraft, such as the tiltrotor experiments by Johnson (Ref. 8) or the numerical investigation by Yemenici (Ref. 9), only focus on the reduction of performance when positioned inboard of a leader wake, rather than the possible improvements outboard of the wake. However, research as early as 1954 shows the similarity between the rotary-wing and fixed-wing far wake and thus indicates that the formation flight mechanism may be applicable. Particularly the investigation by Heyson and Katzoff (Ref. 10) is well-known, showing the development of a longitudinal vortex pair in the rotor wake in forward flight and therefore an outboard upwash region similar to that in fixed-wing wakes. In fact, Heyson and Katzoff suggest that an equivalent fixed-wing approach yields the best results when simulating the far wake of a rotor, emphasizing the physical similarity.

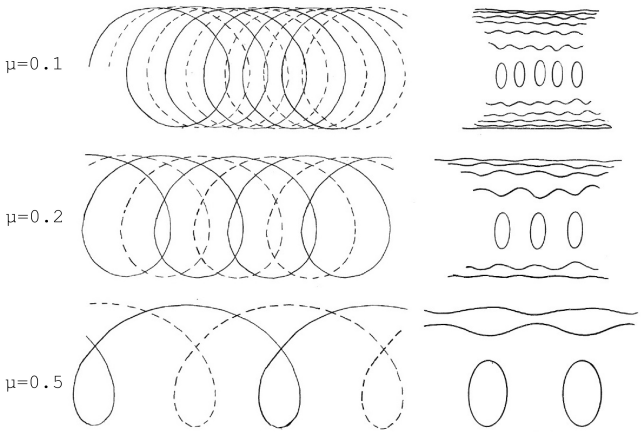

Figure 1: Overlapping tip vortices of a rotor in forward flight (left) decomposed into far wake vortex structures (right). Modified from (Ref. 11)

The problem of formation flight with rotorcraft is notably more complex than for fixed-wing, due to the presence of stall regions and wake asymmetries inherent to rotors in forward flight. It is largely unknown how these phenomena will interact with wake influence of a leader rotor in terms of performance. The measurements by Heyson and Katzoff (Ref. 10) show that the rotor wake has an asymmetric lateral distribution of longitudinal vorticity. Egolf (Ref. 11) proposes how this is qualitatively connected to advance ratio by decomposing tip vortex structures in the far wake into longitudinal and lateral structures, as shown in figure 1. This yields an asymmetric distribution of longitudinal structures at higher advance ratios. Later simulations by Rajagopalan (Ref. 12) and the recent publication by Caprace (Ref. 13) show that the asymmetry of longitudinal vorticity persists into the far wake (shown in figure 2) and particularly that the advancing side vortex is more concentrated, leading to higher upwash velocities outboard of the advancing side, which again agrees with measurements by Heyson and Katzoff (Ref. 10). This leads to the conclusion that rotorcraft formation flight is highly sensitive to alignment and should be aligned on the advancing side for maximum effect. Furthermore, there is a higher potential of wake energy extraction compared to an equivalent symmetric wake. It is therefore hypothesized that rotorcraft may benefit more from formation flight than fixed-wing aircraft can, if aligned on the advancing side of the leader. This hypothesis is further supported by the fact that a rotor can be viewed as a low aspect ratio wing, meaning induced drag has a more dominant contribution to total drag than for most fixed-wing aircraft and thus the impact of induced drag reduction is larger.

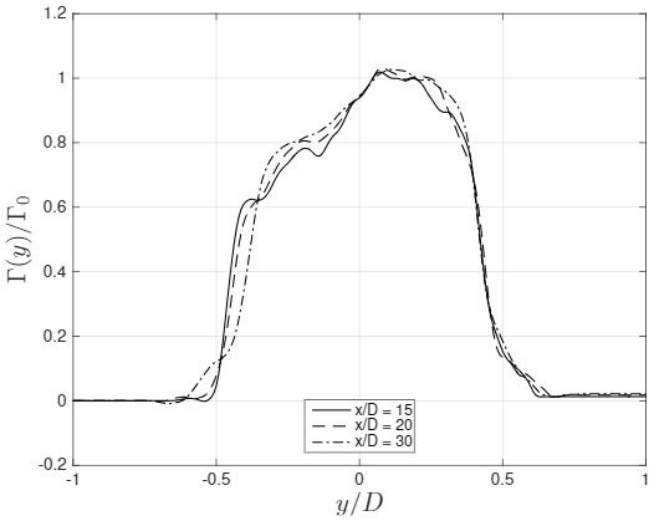

Figure 2: Distribution of circulation in the wake at several downstream locations. (Ref. 13)

METHODOLOGY

As there is no previous research of note, a numerical simulation of Rotorcraft Formation Flight (RFF) is developed in order to investigate the effects of a non-uniform induced velocity field, as generated in the wake of a leading helicopter, on a follower helicopter. The focus of the research is the change in performance of the secondary rotorcraft due to the influence of the wake of the primary rotorcraft. The numerical investigation is supplemented by a wind-tunnel experiment performed on scale-model helicopters. In both cases, a formation of two helicopters is tested at a specified longitudinal distance and lateral and vertical separation is varied in order to map the effects of formation flight with formation configuration. These relative distances are defined in figure 3 for both the numerical and wind-tunnel experiment.

Numerical methodology

The RFF model is built around the follower rotorcraft, the core of which is a rigid multi-body dynamics representation of a UH-60 Black Hawk, utilizing data from Howlett (Refs. 15, 16), Ballin (Ref. 17) and Buckanin (Ref. 18). It is based on the model developed by van Bruchem et al. (Ref. 19),

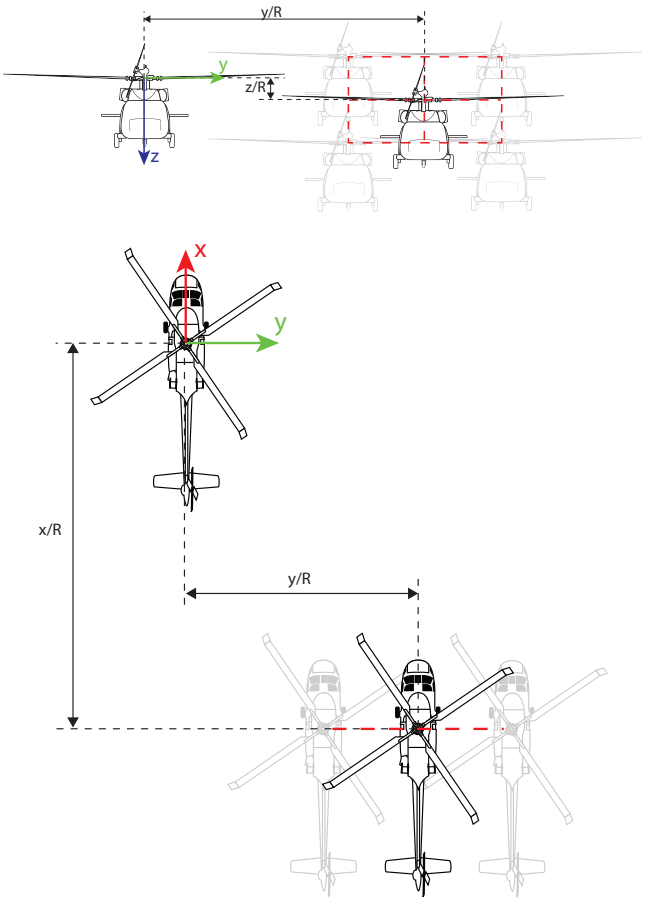

Figure 3: Definition of relative positioning. Blackhawk image source (Ref. 14)

in turn structured according to the approach proposed by Pastorelli et al. (Ref. 20). This includes simulation of both non-rotating and rotating swashplate assemblies. The multi-body dynamics representation is supplemented with a Peters-He inflow model, as described in (Ref. 21), run at 33 states (4 harmonics and 8 radial functions). Rotors are represented as rigid bodies and aerodynamic evaluation is handled by a Blade-Element method at 10 equi-annular sections, with aerodynamic forces and moments taken from lookup tables of experimental NACA 0012 profile data at appropriate Reynolds numbers. Aerodynamic forces and moments on the fuselage are based on the empirical model by Hilbert (Ref. 22). The entire secondary rotorcraft model is controlled by a "trim-by-flight" controller, which autonomously finds the trimmed position in 6 degrees-of-freedom.

The influence of the leader rotorcraft is included on the aerodynamic evaluation of the secondary rotorcraft by the Flat Wake model originally conceived by Baskin et al. (Ref. 23). The implementation is strongly based on the DOWN code developed by NASA, which can be found in (Ref. 24). Wilson (Ref. 25) gives an extensive validation study of this program. In order to ensure agreement further downstream, the present research includes validation of the results of the Flat Wake method using the far wake measurement data from Heyson and Katzoff (Ref. 10). The most important input for the Flat Wake model is the rotor blade vorticity distribution, which is extracted from a baseline solo-flight configuration of the follower rotorcraft model. There is thus no influence of the follower rotor on the leader rotor during simulation, which offers the option of generating a three-dimensional leader wake velocity field out-of-the-loop. Applying a range of $(-6 < x/R < -4; 0 < y/R < 5; -1 < z/R < 1)$ at a resolution of 0.01, the generated velocity field captures the possible blade positions for all simulated formation alignments with negligible loss of accuracy. The model can then interpolate and add the wake velocities to the aerodynamic evaluation points of the follower representation during simulation, which is more efficient than an in-the-loop evaluation of the Flat Wake method for all evaluation points at each time-step. Figure 4 gives a summary of the different modules used in the numerical simulation and the exchange of information between them.

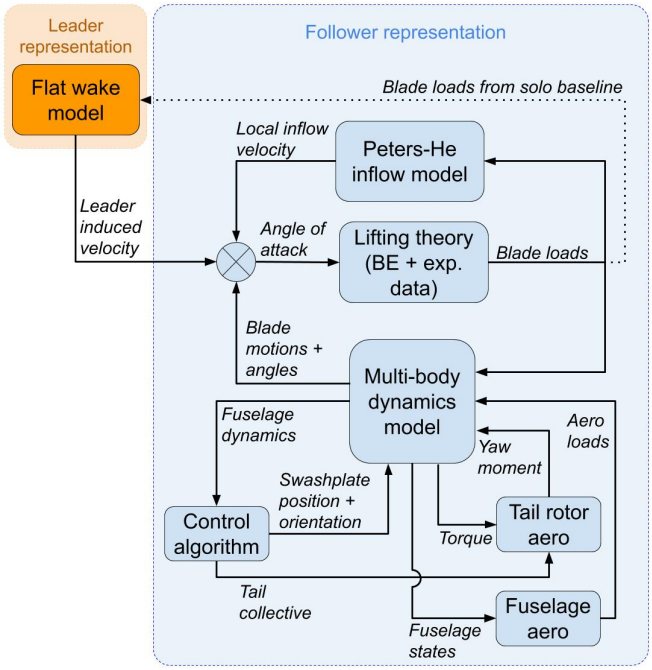

Figure 4: Flowchart of the overall formation modeling. The dotted line represents an out-of-the-loop input based on a baseline calculation.

The resulting numerical model is used to test the effects of formation flight on the secondary rotorcraft in various flight configurations. The primary dataset is taken at 110.8 knots, which corresponds to the maximum range velocity calculated from the secondary rotorcraft model power curve. For the primary dataset, both leader and follower vehicle weight are at roughly MTOW (see table 5). Subsequently, the fuselage mass of the follower rotorcraft is varied between OEW and MTOW in order to observe the effects of payload variations. As the leader experiences no change in these configurations, the same baseline vorticity distribution is used for the Flat Wake method in these scenarios. Furthermore, the velocity of the entire forma-

tion (at MTOW configuration) is varied between 80 and 120 knots in order to observe changes is optimal flight velocity. Here, the vorticity distribution for the Flat Wake method is extracted from a separate baseline for each velocity. In all cases, the position of the follower relative to the leader is varied both vertically and laterally while the longitudinal distance is kept at $x/R = -5$, yielding a two-dimensional map of data. From these the optimal regions in terms of power required, control angles and positional stability are extracted.

The full testmatrix for the numerical simulations is shown in table 1. The first three runs consist of the baselines for the formation flight sequences, evaluating the effects of a variety of fuselage mass and flight speed on the performance of the helicopter in solo flight. The Flat Wake model simulating the leader helicopter is turned off for these simulations. Table 2 yields the masses of the different percentages of fuselage mass.

Run 4 is the primary simulation, yielding the effects of formation flight on the follower helicopter performance at the solo maximum range velocity. Simulations are run for a wide range of horizontal and vertical alignments, as indicated, at intervals of 0.05. Runs 5 and 6 vary follower fuselage mass and formation flight speed respectively, each at intervals of 10. Run 6 utilizes the results of Run 3 as input for the leader wake simulation.

Table 1: Test matrix of numerical simulations.

Run	**FW Model**	**Mass [%]**	**Velocity [kts]**	y/R	z/R
1	Off	100	110.8	-	-
2	Off	70 to 100	110.8	-	-
3	Off	100	80 to 120	-	-
4	On	100	110.8	1 to 3	-0.5 to 0.5
5	On	70 to 100	110.8	1.4 to 2	-0.3 to 0.3
6	On	100	80 to 120	1.4 to 2	-0.3 to 0.3

Table 2: Tested mass percentages and absolute values of follower.

Mass [%]	**Fuselage** [kg]	**Total** [kg]
70	4835	5367
80	5526	6058
90	6216	6748
100	6907	7439

Experimental methodology

The data from the numerical simulations are supplemented with wind-tunnel experiments performed at the Netherlands Defence Academy (NLDA). These involve 3D printed scale-models fitted with variable-rpm fixed-pitch propellers, as shown in figure 5. The fuselages are 3D-printed from polylactic acid (PLA) and are based on the NASA Rotor Body Interaction (ROBIN) model (Ref. 26). They have a length of $28\,cm$, with a hull width of $5.3\,cm$ and a height of $4.5\,cm$. The tail boom is $15\,cm$ long with a diameter of $2.0\,cm$. Measurements are taken at a windtunnel velocity of $9\,m/s$.

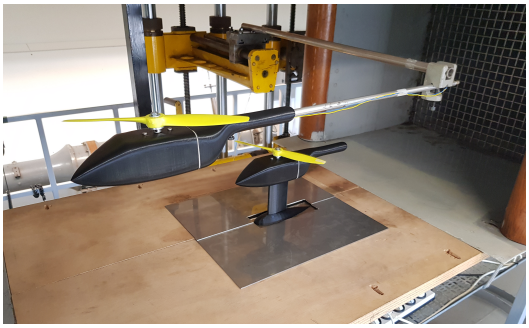

Figure 5: Experimental test setup.

Similar to the numerical simulation, the relative position between follower and leader is varied laterally and vertically while the longitudinal position is kept at $x/R = 2$ due to constraints of the test section. The distribution of measurement points is shown in figure 6. Tachometer data combined with measurements of the forces and moments on the follower model yield rotor rpm, thrust and power, as well as the moments on the body. The rotor thrust is controlled by the rpm setting, which is calculated to deliver $1.8\,N$ of thrust, corresponding to a vertically trimmed flight for the model.

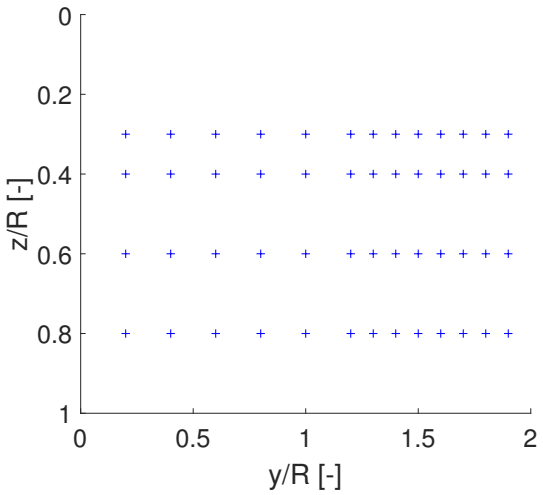

Figure 6: Experimental measurement points.

VERIFICATION AND VALIDATION

In order to place confidence in the results of the RFF model, several steps of verification and validation are performed. The follower representation within the RFF model, being an intricate combination of well-known and validated theories and models, is verified for its computational methods and implementation. Furthermore, the application of the Flat Wake method as a far wake simulation is unprecedented and therefore this implementation is validated.

Follower

The RFF model shares much of its main computational structure and components with the commercial software Flightlab. This software offers a model that is closely related to the UH-60, which is adjusted to mimick the follower representation in the RFF model. The resulting model is used to verify the calculations of the follower representation. Figure 7 shows the angle of attack experienced by one of the blades during one rotation in trimmed condition, showing close correlation in both distribution and magnitude. As the modules of the model all affect each other, rather than being a linear process, this can be viewed as the convergence of all states of the model. This is further exemplified by table 3, which compares the control and body angles in trimmed condition between Flightlab and the formation flight model. This shows close agreement for all parameters except for the tail rotor pitch angle. This is however of no effect to the performance, as the tail rotor is only used to maintain body orientation and has no aerodynamic link to the main rotor.

Variable	Flightlab	RFF model
θ_0 $[deg]$	16.56	15.04
θ_{1s} $[deg]$	5.91	5.82
θ_{1c} $[deg]$	-2.11	-1.31
θ_{0T} $[deg]$	10.21	17.96
β_0 $[deg]$	2.76	1.95
β_{1s} $[deg]$	0.35	-0.39
β_{1c} $[deg]$	-1.80	-2.6
θ_{body} $[deg]$	0.42	1.56
ϕ_{body} $[deg]$	-1.54	-1.47
ψ_{body} $[deg]$	-0.02	0.02

Table 3: Comparison of steady state control, blade and body angles between Flightlab reference and follower model.

The origin of the slight differences between the Flightlab results and the RFF model results can be contributed to the models not being identical. The calculation of the tail rotor forces in Flightlab are based on a Bailey rotor model, whereas the RFF model utilizes a slightly more advanced model (a remnant of the foundation of the model by van Bruchem (Ref. 19). The slight offset in angle of attack distribution on the disk is traced to a difference in the blade center of mass due to the manner of calculating the equi-annular measurement points. Furthermore, it is unclear which version of the Peters-He model is featured in Flightlab, whereas the RFF model uses a basic version as found in (Ref. 21). This may result in slight differences in inflow distribution, which affect all other parameters of the rotor performance. The goal of this verification step is however to verify the correct behavior of the RFF model in trimmed condition, which is found to be confirmed.

Leader

The representation of the leader wake by means of the Flat Wake method by Baskin et al. (Ref. 23) is unprecedented at

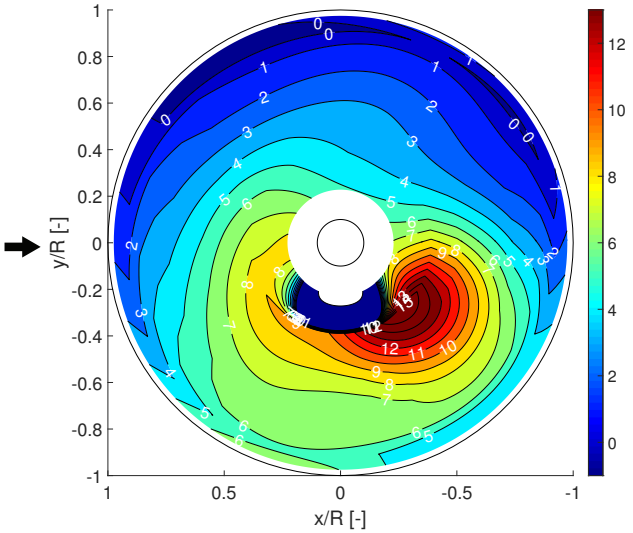

(a) Flightlab

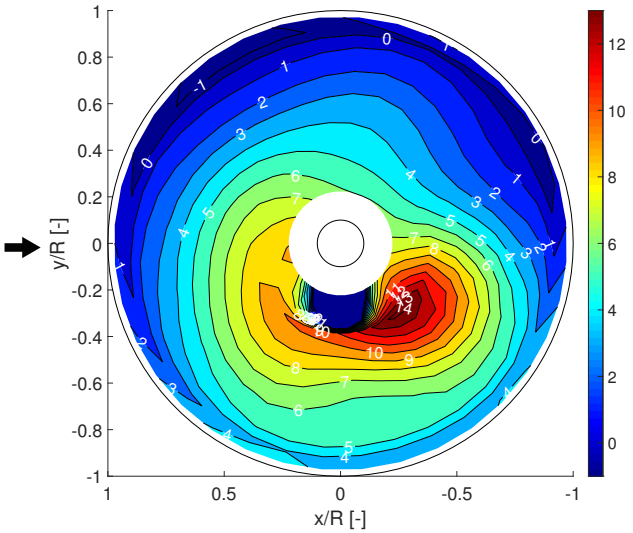

(b) RFF model

Figure 7: Comparison of locally observed angle of attack in degrees on the rotor disk. Arrow indicates freestream direction.

the time of writing of this paper. Though Wilson (Ref. 25) has performed a thorough correlation study on the theory, showing adequate performance considering its fidelity, all data considered is located close to the rotor. This does not guarantee performance of the model when it comes to the far wake development. The same goes for the application of the theory by Takahashi (Ref. 27), who used it to determine the effect of the main rotor on the tail rotor. The present research therefore includes a validation phase of the Flat Wake method at further downstream distances. As data on the far wake aerodynamics of rotorcraft in high speed forward flight is scarce, the dataset of Heyson and Katzoff (Ref. 10) is used for this purpose. This includes measurements of the induced velocity in z-direction at $x/R = -3.14$, which is more than a diameter behind the rotor. Though the numerical simulation is performed at $x/R = -5$, the validation at this distance is deemed adequate based on the knowledge that most of wake deflection

and rollup occurs before this downstream station (Ref. 10).

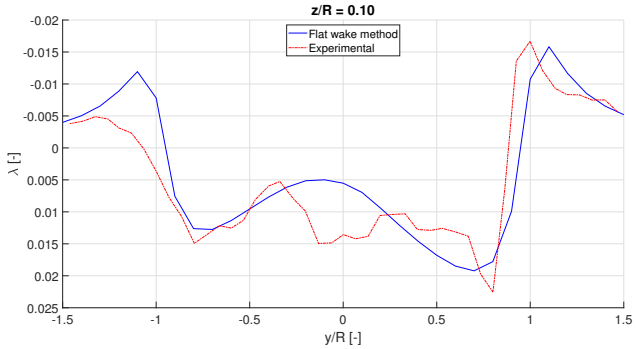

Figure 8: Vertical induced velocity λ as predicted by the Flat Wake method versus measurements. $x/R = -3.14$. Axes defined according to figure 3.

Figure 8 shows a comparison of the vertical induced velocity, which is the main variable of importance to formation flight effects, as predicted by the Flat Wake method compared to measurements made by Heyson and Katzoff (Ref. 10). These are taken at a vertical position of $z/R = 0.10$ and include outboard lateral positions on both the advancing (right) and retreating (left) sides. It shows that the Flat Wake method is able to predict the general trend of the values, though local variations are not captured. The asymmetry of induced velocity between advancing and retreating sides is clearly visible in both the predicted and measured data. The correlation of the Flat Wake prediction is notably better on the advancing side than the retreating side. This is seen in comparisons at other stations as well, but as the formation is aligned on the advancing side, this poses no issue to the validity of the model for the present research.

RESULTS

This section presents the results of the completed rotorcraft formation flight model, in which the multi-body dynamics based follower model is subjected to the effects of the leader wake. It includes analyses of the effects of formation flight on power required, trim controls/moments and static positional stability.

Numerical simulation

In contrast to the fixed-wing formation flight research, where aerodynamic benefit of formation flight is found from the induced drag, the effect of formation flight on the performance of rotorcraft is best viewed from the main rotor power required. The main result of the numerical simulation is therefore the fraction of main rotor power required in formation compared to the baseline value at various positions of formation flight. This is supported by findings on control and stability, as well as the effects of various of payload mass and formation flight velocity. Because the RFF model includes full aerodynamic drag of both blades and fuselage in its simulation, the main rotor power required can be interpreted as proportional to total aircraft drag in fixed-wing formation flight studies.

Power required Figure 9 shows the fraction of follower main rotor power required in formation vs solo flight. The axes represent the lateral and vertical distance between the rotor hubs of leader and follower rotor, as defined in figure 3. Figure 9 shows a maximum power reduction of about 20%, which is a significantly higher number than observed in fixed-wing formation flight research, where total aircraft drag reductions typically ranges between 10 to 15%.

The optimum position in terms of benefit to main rotor power required is indicated in figure 9 and found to be $(y/R, z/R) = (1.65, 0)$. This means that a part of the follower disk area is positioned in the downwash region of the leader wake. Although it may be expected that this would lead to a reduction in performance, figure 10 illustrates how the circular disk area benefits more from an alignment in which the tip experiences downwash rather than upwash. In figure 10a, the tip is aligned with the leader disk vortex, resulting in upwash on the entire disk. The maximum of this upwash is however only applied to a small area on the edge of the follower disk. Figure 10b represents the optimal alignment, where the tip experiences some downwash, but the peak of the upwash is applied to a much larger area of the disk. This results in a higher reduction in main rotor power required. This indicates that the precise optimal lateral alignment is dependent on operating conditions of the disk and rotor geometry, but should always be expected to feature some overlap.

Control angles Figure 11 shows the same two-dimensional maps as given in figure 9, but for the trim control variables as a fraction of their baseline value. A few notable observations can be made. First of all, the collective angle map is similar to the power fraction map, but their minima do not coincide. This shows the dependency of the other control variables on the performance. The longitudinal cyclic is shown to have a strong lateral gradient, much more so than the lateral cyclic. This shows rotorcraft are mainly affected in pitch characteristics when in formation flight. This can be contributed to the occurrence of phase lag in articulated rotors. The upwash from the leader wake is most effective on the retreating side of the follower disk, which translates into forces and moments applied on the rotorcraft with a roughly 90-degree phase delay, thus primarily affecting pitch behavior.

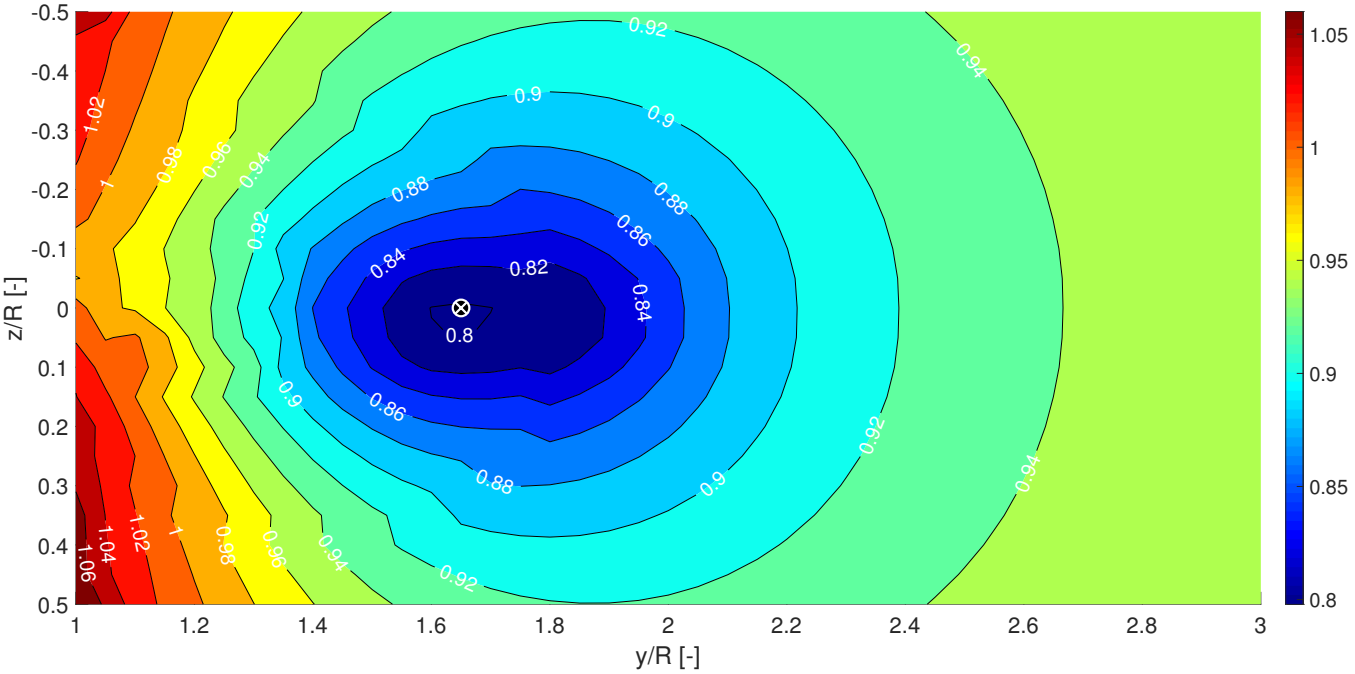

Figure 9: Main rotor power required in formation as a fraction of the baseline value ($P_{req,BL} = 677\,kW$). Indicator gives location of minimum power fraction. Numerical simulation.

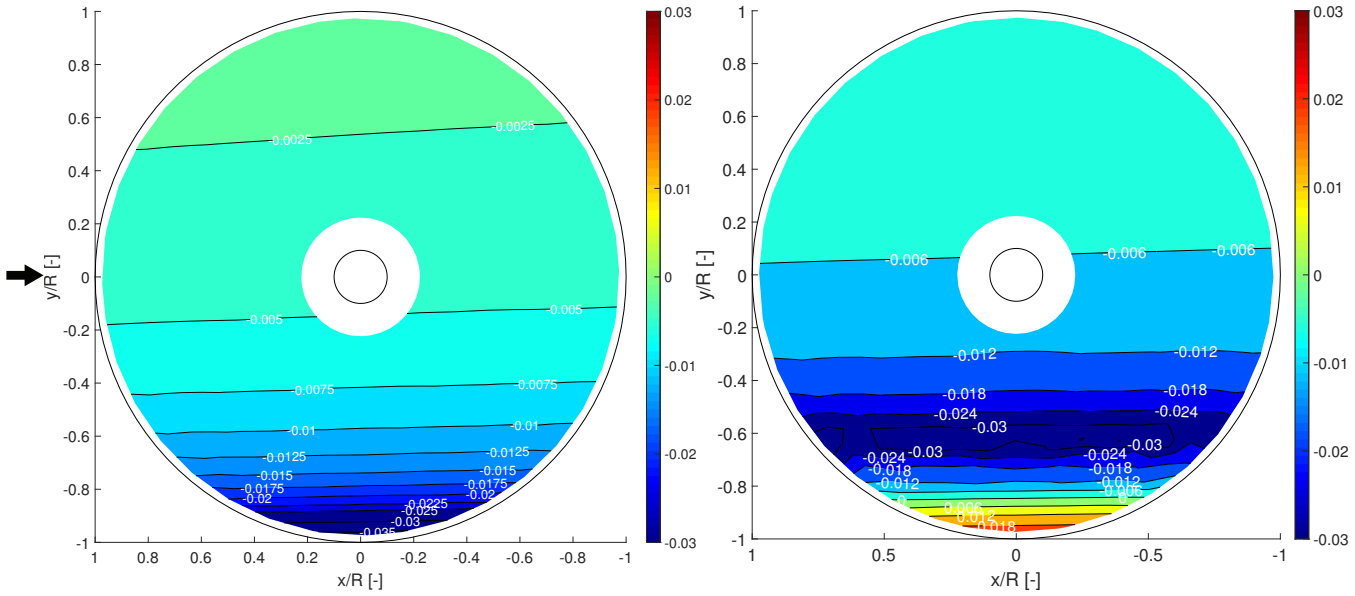

(a) $(x,y,z) = (-5R, 2R, 0)$ (b) $(x,y,z) = (-5R, 1.65R, 0)$

Figure 10: Leader induced vertical inflow λ on the follower disk for "tip-to-tip" alignment (left) versus optimal alignment (right). Arrow indicates freestream direction. Numerical simulation.

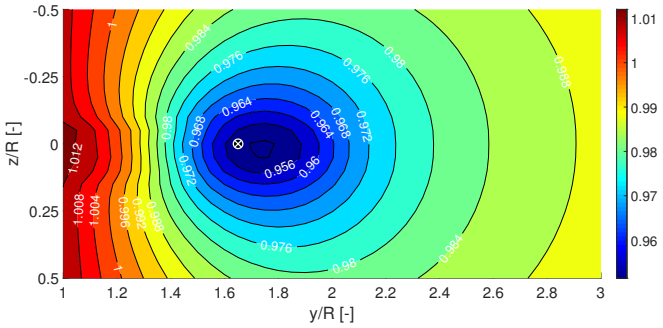

(a) Collective angle

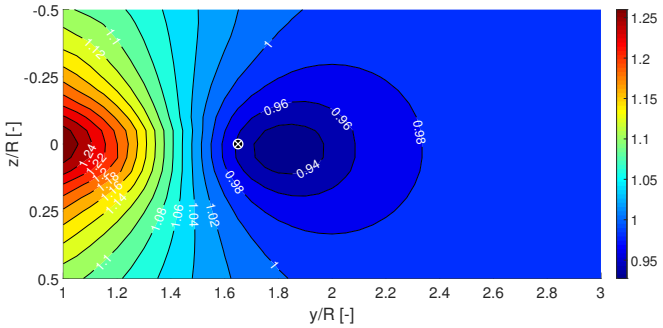

(b) Longitudinal cyclic

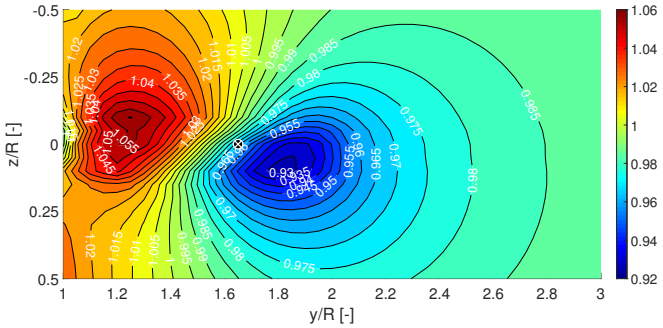

(c) Lateral cyclic

Figure 11: Follower trim angle fractions as a function of alignment. Indicator gives location of minimum power fraction. Numerical simulation.

Table 4: Summary of required power and control data in and out of formation. Numerical simulation. Limits are taken from Howlett (Ref. 15)

	Power	**Collective**	**Lat. cyclic**	**Long. cyclic**
Magnitude				
	$[kW]$	$[deg]$	$[deg]$	$[deg]$
Max.	725	15.24	-1.34	7.38
Min.	540	14.31	-1.22	5.40
Solo	677	15.04	-1.31	5.82
Limits	-	9.9:25.9	-8:8	-12.5:16.3
Fraction				
	$[-]$	$[-]$	$[-]$	$[-]$
Max.	1.071	1.013	1.060	1.269
Min.	0.798	0.951	0.928	0.927
Position				
	$(y/R, z/R)$	$(y/R, z/R)$	$(y/R, z/R)$	$(y/R, z/R)$
Max.	(1,0.5))	(1,-0.05)	(1.8,0.1)	(1,0)
Min.	(1.65,0)	(1.7,0)	(1.25,-0.1)	(1.8,0)

In general, the effect on the control angles required for trim is found to be mild. Though the maximum deviation of the longitudinal cyclic is 25%, this only occurs at the very edge of the range of alignments and still translates to a control setting well within the limits of the control system. The other control angles show even less deviation from their baseline value, as summarized together with the power data in table 4. A final notable observation is that at the optimal position in terms of power, all control angles are reduced compared to their baseline value, meaning the formation flight effects counteract the moments experienced in solo flight.

Static positional stability Taking the gradients from the control angle maps also yields insight into the static positional stability of the follower in the formation. The static positional stability is based on the moments that would act on the follower in trimmed condition under the influence of a small positional disturbance, without adjusting its controls. As the data is obtained in lateral and vertical direction, the ability of the follower to maintain its position in y- and z-directions can be found. The stability in y-direction is dependent solely on the lateral cyclic control and can be considered stable if the gradient with respect to y is negative, as given by equation (1). This would mean that any disturbance in lateral position without adjusting control settings would induce a moment counteracting the disturbance.

$$\frac{\delta\theta_{1c}}{\delta y} > 0 \quad (1) \qquad \frac{\delta\theta_{1s}}{\delta z} < 0 \quad (2) \qquad \frac{\delta\theta_{0}}{\delta z} > 0 \quad (3)$$

The stability in z-direction is dependent on both the collective and longitudinal cyclic controls, according to equations (3) and (2) respectively. Complete positional stability in z requires both collective and longitudinal cyclic contributions to be stable. In case of a single stable parameter, stability is conditional on the relative influence of each parameter, which is not evaluated in the present research. Figure 12 indicates the positional stability of the follower at each position, plotted over the power fraction map.

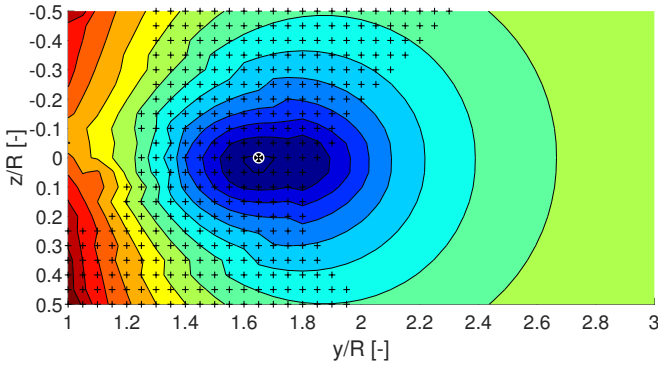

(a) Stability in y - Lateral cyclic

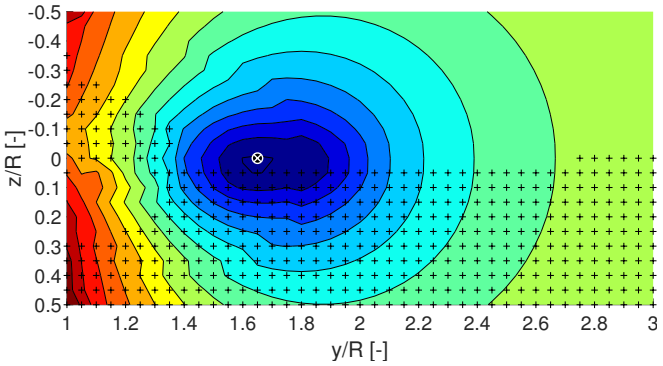

(b) Stability in z - Collective

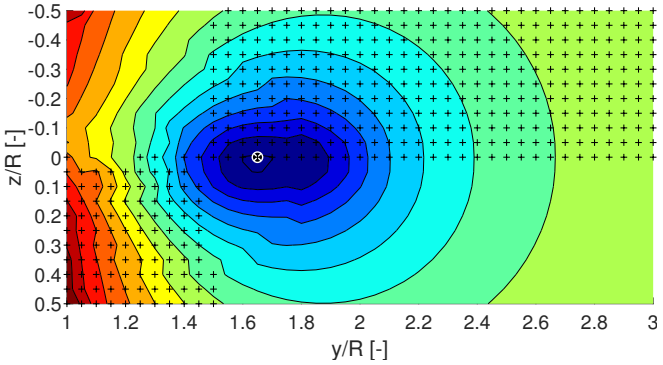

(c) Stability in z - Longitudinal cyclic

Figure 12: Static positional stability in y- and z-direction of follower plotted over the main rotor power fraction. (+) marks stable conditions, unmarked areas are unstable. Minimum power fraction location is indicated. Numerical simulation.

Most of the region featuring a reduction in power is shown in figure 12a to be stable in y-direction . As the follower is positioned further outboard, the position becomes unstable. The presented data does not indicate the severity of the instability, though from the small gradient of the lateral cyclic angle found in figure 11c it is safe to assume that any instability is of mild characteristic. The stability of the optimum position strongly contrasts findings in fixed-wing formation flight, such as presented by Veldhuis and Voskuijl (Ref. 28), where the optimum is found to be unstable with respect to every control direction.

The stability in z-direction is found to be conditional for nearly every position. This means that the actual stability in z is dependent on the relative contributions of collective and longitudinal cyclic gradients. As with the lateral cyclic however, the gradients observed in the control maps of figure 11a and 11b are small, particularly with respect to z-direction, and instabilities are therefore expected to be mild.

Mass variations The follower fuselage mass is varied between 70 and 100 % of the primary simulation value, corresponding roughly to OEW and MTOW respectively. These results can be used to determine the effects of variable payload between leader and follower. Leader is kept at constant mass (equal to the 100% follower mass setting) for all simulations. The simulations are carried out for a range of lateral and vertical positions similar to the primary simulation. Table 5 summarizes the maximum achieved reduction in power required for each mass variation, along with the corresponding position.

Table 5: Summary of effects of changing follower fuselage mass, $\mu = 0.26$. Numerical simulation.

Mass [%]	70	80	90	100
$\Delta P_{req,MR}$ follower [%]	17.5	19.5	21.1	20.3
Position $(y/R, z/R)$	(1.5,0)	(1.6,0)	(1.7,0)	(1.65,0)

The correlation of follower fuselage mass and achieved power reduction in formation is shown to be non-linear, with an optimum at 90% follower fuselage mass. Furthermore, the optimum position moves inboard as achievable power reduction decreases. These observations are likely tied to the stall region on the retreating blade, which is partly dependent on the collective control and thus on the required lift. Lower lift requirements will result in a less pronounced stall region, changing the balance of the circular disk area effect (figure 10) because of more effective root area. This allows for a more inboard position before the downwash on the tip region outweighs the upwash in the inboard regions. The non-linearity with the mass percentage indicates however that this is not the only contribution.

Velocity variations Changing the velocity of the formation reveals that the follower can achieve profoundly higher power reductions as the formation velocity decreases. This follows from the increase in vertical wake velocity of the leader associated with the lower forward velocity, allowing for a larger benefit to the follower. Table 6 gives the minimum main rotor power required for the solo baseline, follower in formation and average of the formation. It shows that the follower power required in formation equals $359.3\,kW$ at a flight speed of 80 knots, which accounts to a reduction of 34% compared to the baseline. When averaged over both rotorcraft in the formation, the maximum achievable power reduction is found to be 17% at 80 knots.

Table 6: Main rotor power required for varying flight speeds at a relative position of $(y,z) = (1.65R, 0)$. Numerical simulation.

Velocity $[kts]$	80	90	100	110	120
Advance ratio $[-]$	0.187	0.211	0.234	0.257	0.281
$P_{req,MR}$ (Solo) $[kW]$	544.7	579.1	625.6	686.4	768.3
$P_{req,MR}$ (Follower) $[kW]$	359.3	409.4	472.1	537.8	636.5
$P_{req,MR}$ (Averaged) $[kW]$	452.0	494.3	548.8	612.1	702.4

At a formation flight speed of 80 knots, the leader performance is deteriorated however, which offsets some of the power reduction experienced by the follower. The effects of this are particularly clear when comparing the maximum

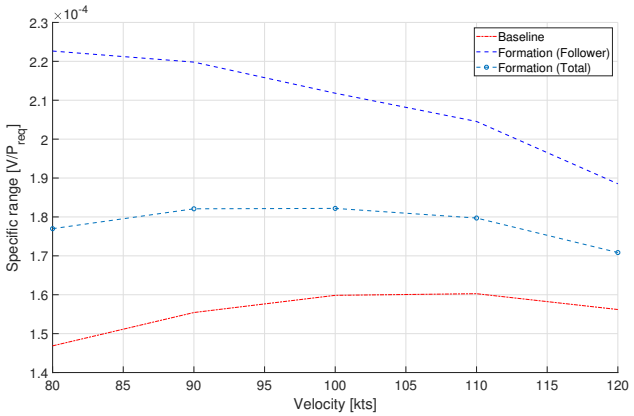

Figure 13: Specific range curves for the baseline, follower in formation and total formation (averaged). Numerical simulation.

range velocity of baseline, follower in formation and the formation average. Taking the power as directly proportional to the fuel consumption, the specific range can be estimated by dividing the flight velocity by the power required. This yields figure 13, which shows how the maximum range velocity is changed by formation flight. The average of the total formation has a maximum around 100 knots, compared to roughly 110 knots for the solo baseline. Reducing the velocity further increases the specific range of the follower, but results in larger losses for the leader (which performs equal to the solo baseline). The change in optimum flight speed for a formation as a whole is notably also found for fixed wing aircraft, as reported in (Ref. 29).

Wind-tunnel experiment

The results from the wind-tunnel experiment can be reported in a similar manner to the numerical results. This includes main rotor power required fraction, rolling and pitching moments (since there are no control angles for the rigid scale-model rotors) and positional stability.

Power required Figure 14 shows a similar dataset to figure 9 of the numerical results, namely the main rotor power required of the follower in formation as a fraction of the baseline. The minimum power required is found to be 49% of the baseline value at $y/R = 1.3$ and $z/R = 0.6$, corresponding to a power reduction of 51%. It should be noted here that the parasitic power requirement is not included in the measurements due to the experimental setup. Using standard division of contributions to the power required corresponding to the tested advance ratio, as found in Prouty (Ref. 30), an estimation is made that the equivalent total power reduction would be about 24%. The non-uniformity of the power fraction map is likely contributed to the non-uniform distribution of the vortices at this longitudinal station of the leader wake, as can be inferred from the simulations by Caprace (Ref. 13).

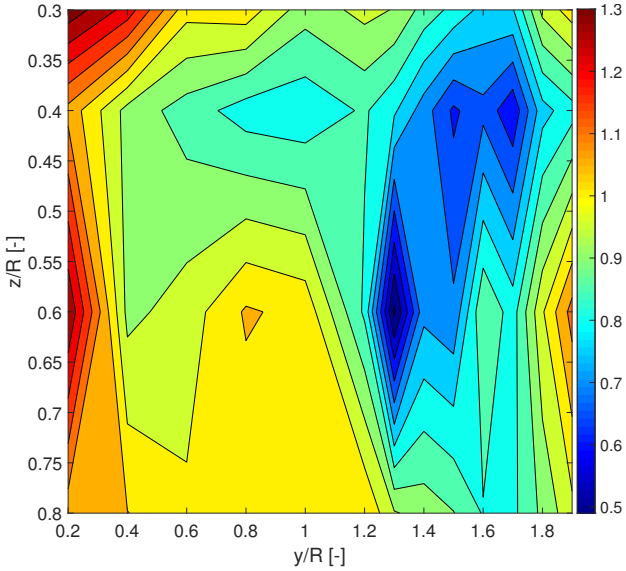

Figure 14: Measured main rotor power required in formation as a fraction of the baseline. $\mu = 0.36$. Wind-tunnel measurement.

Pitch and roll moments Figure 15 shows the change in measured pitching and rolling moments of the follower in formation from their baseline values ($0.0295\,Nm$ and $-0.0682\,Nm$ respectively). The observed variation of pitching moment can be explained well by taking into account two contributions to the change. The first is the change in pitching moment due to the change of power required. As the power required scales with the rpm of the rotor, a lower power required will reduce the overall moment experienced by the rotor. The lateral variation of pitch moment can be primarily contributed to this effect. The vertical variation of the pitching moment, which is primarily present between lateral coordinates $y/R = 1$ and $y/R = 1.8$, can be contributed to the immersion of the follower rotor in the downwash of the leader. Considering the downwash of the leader as a skewed cylinder and taking into account the short longitudinal distance between rotors, the front half of the follower rotor is immersed in the downwash cylinder as it is moved in positive z-direction. This causes additional pitch down moment, increasing the difference with the (pitch-up) baseline value.

The rolling moment can be dissected similarly, though it is slightly more complex. We can again identify a contribution to the lateral variation and the vertical variation. The first is the distribution of downwash and upwash on the rotor. Considering the wake of the leader as a flat vortex sheet, such as in the numerical simulation, the point of maximum effect of formation flight on the rolling moment should be expected to be seen at $y/R = 1$. As the follower moves from right to left, the change in rolling moment should be expected to decrease as it approaches the minimum, after which is should increase again, as is observed in figure 15b. Vertical variation can again be contributed to immersion in the streamtube of the leader, as the left-front quadrant of the follower rotor will experience

more downwash with increasing z-coordinate. For small y-coordinates, the difference between left en right quadrants is reduced and thus the rolling moment becomes less dependent on the lateral station.

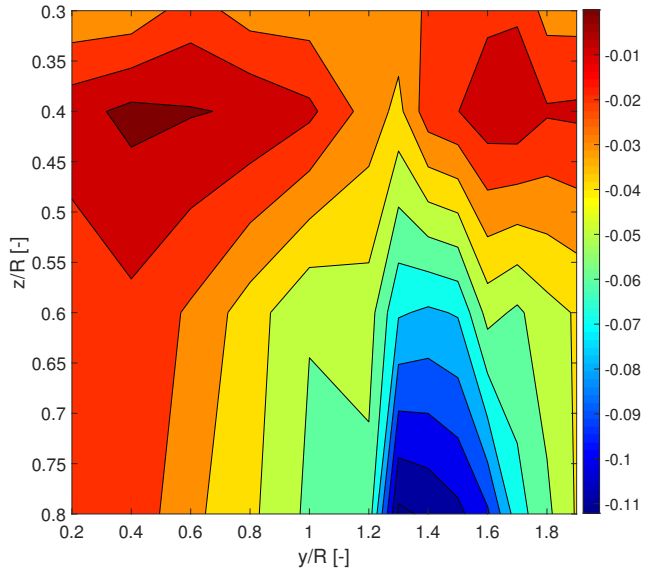

(a) Pitch moment [Nm]

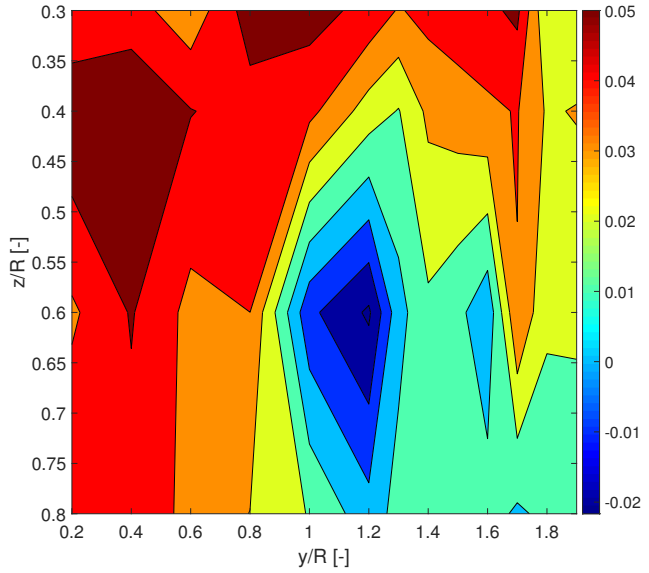

(b) Rolling moment [Nm]

Figure 15: Measured change in moments experienced by the follower in formation. $\mu = 0.36$. Wind-tunnel measurement.

However, since the rpm scales with the power required and the rotors are fixed, there is a strong dependency of the rolling moment on the power required. This is much stronger than the dependency of the pitching moment on the power required, due to the forward velocity. It should also be noted that the analysis of figures 15a and 15b reveal an essential difference between the articulated rotor of the follower in the numerical simulation, which is primarily affected by formation flight in its pitching moment due to phase lag, whereas the fixed rotors used in the experiment do not experience phase lag and are thus affected strongly in their rolling moment.

Static positional stability From figures 15a and 15b an estimate of the static positional stability in y and z can also be deduced. Stability in y and z are respectively considered stable if the change in pitch and roll moment counteracts a positional disturbance. Considering normal rotor conventions, this means that the roll moment gradient has to be negative, while the pitch moment gradients has to be positive, as given in equation (4) for roll and equation (5) for pitch behavior.

$$\frac{\delta M_\phi}{\delta y} < 0 \qquad (4) \qquad\qquad \frac{\delta M_\theta}{\delta z} > 0 \qquad (5)$$

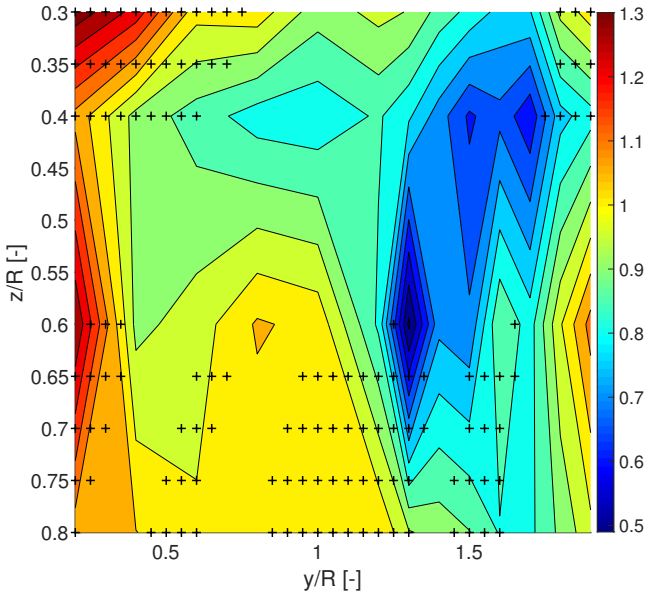

(a) Stability in z

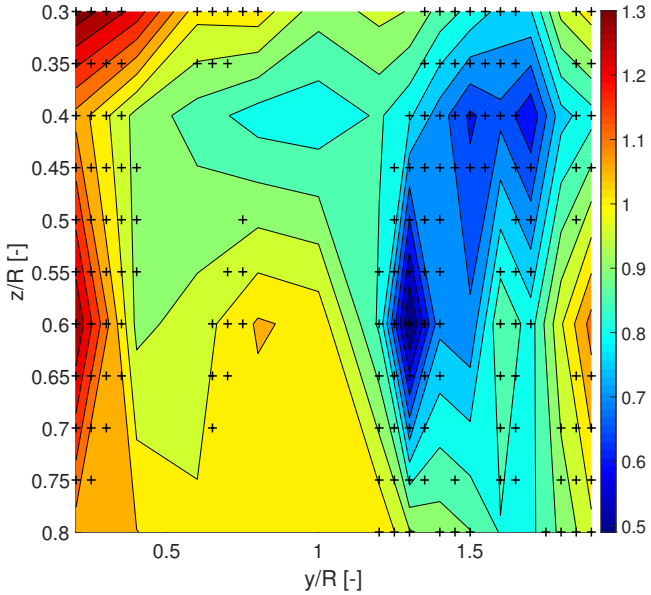

(b) Stability in y

Figure 16: Stability in z- and y-direction plotted over power required fraction. $\mu = 0.36$. Stable areas denoted with (+) markers. Wind-tunnel measurement.

Taking the gradient of the roll and pitch moments of figure 15 and applying equations (4) and (5) then yields the stability regions as shown in figure 16a and 16b for y- and z-direction respectively. The markers indicate stable positions. It shows that stability in y-direction is present for most of the region associated with the lowest power requirements. The z-direction shows stability for most of the area below the minimum power required point, while the region above it is unstable. This is similar to the dependency of stability in z-direction on collective, as seen in the numerical simulations. No strong conclusions can be tied to these observations, but they only showcase a method for determining positional stability in formation flight.

CONCLUSIONS AND RECOMMENDATIONS

This research investigated the validity of utilizing formation flight principles to reduce main rotor power required of rotorcraft. A numerical model representing two UH-60 helicopters in echelon formation was created. The numerical simulation was supported by an independent wind-tunnel experiment of two scale-model helicopters.

The following main conclusions can be drawn from this research:

- Both numerical and wind-tunnel experiments yield a positive proof of concept for the use of formation flight for aerodynamic benefit with rotorcraft.
- Due to the asymmetric nature of the rotor wake, rotorcraft have a higher potential for aerodynamic benefit than conventional fixed-wing aircraft.
- At the solo maximum range velocity, the numerical simulation yields a maximum achievable reduction of total power required for the follower of 20%. Compensating the wind-tunnel results for the absence of parasitic drag yields about 24% of maximum total power required reduction.
- In the numerical simulation, the optimal alignment in formation resulted in lower required trim settings for the follower compared to solo flight.
- According to the numerical results, the maximum range flight speed when considering the formation as a whole is reduced compared to solo flight.
- In the numerical experiment, the follower is positionally stable in y-direction and conditionally stable in z-direction in the region of maximum power reduction.
- In the wind-tunnel experiment, the results shows a more distributed area of strong power reduction. The positional stability characteristics are similar to the numerical results.

Recommendations

The research presented in this document is a first step in understanding the principles of formation flight as applied to rotary wing vehicles. The authors give several recommendations for the continued pursuit of this subject.

- In order to investigate the effects of 3D flow phenomena, the RFF model should be fitted with a more advanced leader wake simulation. A vortex particle method would lend itself for this purpose, in order to overcome the difficulty of numerical diffusion and computational cost for the far wake region.
- Another important aerodynamic improvement would be to include fuselage interference effects. Both the effect of the leader wake on the fuselage as well as the fuselage on the main rotor would be of interest.
- The recent research by Caprace (Ref. 13) has uncovered the concept of far wake strengthening, which seems to be supported indirectly by other sources. This phenomenon may raise achievable drag reductions at larger longitudinal separations significantly and warrants further investigation.
- The collected numerical data on the variations of fuselage mass and formation velocity can be used to perform a first estimate of mission specific achievable benefits of formation flight.
- Aerodynamic measurements of two rotors in formation can yield insight into the wake interaction and whether the wake asymmetry between advancing and retreating side persists for larger formations.
- The non-linear behavior of achievable power reduction with follower fuselage mass warrants additional investigation.

For further inquiries on the available data or further specification of the models, please contact the authors:
Ramon Duivenvoorden (ramonduivenvoorden@gmail.com),
Mark Voskuijl (M.Voskuijl@mindef.nl).

REFERENCES

1. Wieselberger, C., "Beitrag zur Erklärung des Winkelfluges einer Zugvogel," *ZFM*, Vol. 5, 1914, pp. 225–229.
2. Lissaman, P. B. S., and Shollenberger, C. A., "Formation Flight of Birds," *Science*, Vol. 168, 1970, pp. 1003–1006.
3. Hummel, D., "Recent Aerodynamic Contribution to Problems of Bird Flight," ICAS 1978, 1978.

4. Hummel, D., "Aerodynamic aspects of formation flight in birds," *Journal of Theoretical Biology*, Vol. 104, 1983, pp. 321–347. DOI: 10.1016/0022-5193(83)90110-8

5. Ning, A., Flanzer, T. C., and Kroo, I. M., "Aerodynamic Performance of Extended Formation Flight," *Journal of Aircraft*, Vol. 48, (3), 2011, pp. 855–865. DOI: 10.2514/1.C031046

6. Ning, S. A., Kroo, I., Aftosmis, M. J., Nemec, M., and Kless, J. E., "Extended Formation Flight at Transonic Speeds," *Journal of Aircraft*, Vol. 51, (5), sep 2014, pp. 1501–1510. DOI: 10.2514/1.C032385

7. Bieniawski, S. R., Clark, R. W., Rosenzweig, S. E., and Blake, W. B., "Summary of flight testing and results for the formation flight for aerodynamic benefit progam," 52nd Aerospace Sciences Meeting, 2014.

8. Johnson, W., "A History of Rotorcraft Comprehensive Analyses," AHS 69th Annual Forum, 2013.

9. Yemenici, O., Uzol, N. S., and Uzol, O., "Investigation of rotor-rotor interactions for two helicopters in forward flight using free-vortex wake methodology," 28th AIAA Applied Aerodynamics Conference, 2010.

10. Heyson, H. H., and Katzoff, S., "Induced Velocities Near a Lifting Rotor with Non-Uniform Disk Loading," Technical report, National Advisory Committee for Aeronautics, Langley Field, Va., 1957.

11. Egolf, T. A., *An Analytical and Experimental Study of Farfield Rotor Wake Geometry and Velocity*, Master of science, Pennsylvania State University, 1973.

12. Rajagopalan, R. G., and Mathur, S. R., "Three dimensional analysis of a rotor in forward flight," *Journal of the American Helicopter Society*, Vol. 38, (3), jul 1993, pp. 14–25.

13. Caprace, D.-G., Buffin, S., Duponcheel, M., Chatelain, P., and Winckelmans, G., "Large Eddy Simulation of Advancing Rotor for Near to Far Wake Assessment," 43rd European Rotorcraft Forum, 2017.

14. FOX 52, "UH-60A Blackhawk illustration," https://commons.wikimedia.org/w/index.php?curid=44705055, [Online; accessed May 2019; CC BY-SA 4.0].

15. Howlett, J., "UH-60A Black Hawk Engineering Simulation Program: Volume I - Mathematical Model," NASA Contractor Report 66309, 1981.

16. Howlett, J., "UH-60A Black Hawk Engineering Simulation Program: Volume II -Background Report," Technical report, National Aeronautics and Space Administration, 1988.

17. Ballin, M. G., "Validation of a Real-Time Engineering Simulation of the UH-60A Helicopter," NASA Technical Memorandum 88360, 1987.

18. Buckanin, R. M., Reynolds, T. L., Kelly, W. A., Lockwood, R. A., Webre, J. L., and Cason, R. W., "Level Flight Performance Evaluation Of The UH-60A Helicopter With The Production External Stores Support System And Ferry Tanks Installed," Technical report, U.S. Army Aviation Engineering Flight Activity, St. Louis, Mo, 1986.

19. Voskuijl, M., Van Bruchem, B.-J., and Van Liempt, M., "Helicopter drive train load alleviation in hover by nonlinear control," AHS International 74th Annual Forum & Technology Display, 2018.

20. Pastorelli, S., Battezzato, A., and Mattiazzo, G., "Fly-by-wire Control of a Helicopter: Multibody Main Rotor Model," 26th International Congress of the Aeronautical Sciences, 2008.

21. Peters, D. A., and He, C. J., "Finite State Induced Flow Models Part II: Three-Dimensional Rotor Disk," *Journal of Aircraft*, Vol. 32, (2), 1995, pp. 323–333(11). DOI: 10.2514/3.46719

22. Hilbert, K. B., "A Mathematical Model of the UH-60 Helicopter," NASA Technical Memorandum 85890, 1984.

23. Baskin, V. E., Vil'dgrube, L. S., Vozhdayev, Y. S., and Maykapar, G. I., *Theory of the lifting airscrew (NASA Technical Translation)*, National Aeronautics and Space Administration, Washington, D.C., nasa tt f- edition, 1976, p. 481.

24. Wilson, J. C., "Technical Memorandum 104139: User's Guide For A "Flat Wake" Rotor Inflow/Wake Velocity Prediction Code, "DOWN"," Technical report, National Aeronautics and Space Administration, Hampton, Virginia, 1991.

25. Wilson, J. C., "Experimental Evaluation of a Flat Wake Theory for Predicting Rotor Inflow-Wake Velocities Aeroflightdynamics Directorate-A VSCOM DT iC TAB 0 JRPO-Langley Availability Codes Aval atld or," NASA AVSCOM Technical Memorandum 4334, 1992.

26. Freeman, C. E., and Mineck, R. E., "Fuselage Surface Pressure Measurements of a Helicopter Wind-Tunnel Model with a 3.15-Meter Diameter Single Rotor," NASA Technical Memorandum 80051, 1979.

27. Takahashi, M. D., "A Flight-Dynamic Helicopter Mathematical Model with a Single Flap-Lag-Torsion Main Rotor," NASA Technical Memorandum 102267, 1990.

28. Veldhuis, L., Voskuijl, M., and Fransen, B., "Formation Flight - Fine-tuning of Theoretical Performance Prediction," 51st AIAA Aerospace Sciences Meeting including the New Horizons Forum and Aerospace Exposition, 2013. DOI: doi:10.2514/6.2013-961

29. Voskuijl, M., “Cruise Range in Formation Flight,” *Journal of Aircraft*, Vol. 54, (6), 2017, pp. 1–8. DOI: 10.2514/1.C034246

30. Prouty, R. W., *Helicopter Performance, Stability, and Control*, Krieger Publishing Company, Malabar, Florida, fourth edition, 2002.